DOI: 10.1021/ma101006e

Macromolecules
ARTICLE

Competitive Growth of α- and β-Crystals in β-Nucleated Isotactic Polypropylene under Shear Flow

Yan-Hui Chen,[†] Yi-Min Mao,[‡] Zhong-Ming Li,*[,†] and Benjamin S. Hsiao*[,‡]

[†]*College of Polymer Science and Engineering and State Key Laboratory of Polymer Materials Engineering, Sichuan University, Chengdu 610065, China, and* [‡]*Department of Chemistry, Stony Brook University, Stony Brook, New York 11794-3400*

Received May 6, 2010; Revised Manuscript Received July 16, 2010

ABSTRACT: It has been well established that, although both shear flow and β-nucleating agent could separately induce β-crystals in isotactic polypropylene (iPP) in an efficient manner, their combination in fact depressed the content of β-crystals when compared with quiescently crystallized β-nucleated iPP. In the current study, in-situ synchrotron wide-angle X-ray diffraction (WAXD) and small-angle X-ray scattering (SAXS) measurements were performed to investigate this behavior. The WAXD data obtained were quantitatively analyzed to determine the independent contributions of applied shear flow and added β-nucleating agent in terms of nucleation stage and subsequent α- and β-crystal growth stage. In the nucleation stage, the addition of β-nucleating agent increased the amount of β-nuclei, while the application of shear flow and the interactions between shear and β-nucleating agent enhanced the amount of α-nuclei (the amounts of α- and β-nuclei were in the same order of magnitude). As a result, in the initial crystallization, α- and β-crystals grew competitively, causing simultaneously increments of α- and β-crystals. However, in the growth stage, the growth rate of β-crystals was faster than that of α-crystals where the epitaxial growth of β-crystals on α-crystals also occurred (due to more favorable isothermal crystallization temperature for β-crystal growth). Consequently, the content of β-crystals became dominant in the limited growth space; however, it was still less than that formed from the quiescent isothermal crystallization of β-nucleated iPP. As the shear rate increased, more shear-induced α-nuclei were formed, further decreasing the amount of β-crystals. Nevertheless, when shear and β-nucleating agent coexisted, β-crystals emerged earlier than α-crystals. The SAXS results indicated that the combination of shear and β-nucleating agent changed the stacking manner of molecular chains, so that the long period of sheared, β-nucleated iPP was comparable to that of quiescently crystallized iPP.

Introduction

Isotactic polypropylene (iPP) is a polymorphic material having at least four modifications: α, β, γ, and smetic.[1−4] The α-form is a thermodynamically stable phase and has good mechanical strength, resulted from the cross-hatched lamellar morphology and compact stacking of molecular chains. However, its toughness is quite poor at low temperatures. The β-form is a thermodynamically metastable phase, which can be obtained by special conditions, such as in the presence of certain heterogeneous nucleating agents,[5−9] crystallization in a temperature gradient,[10,11] or crystallization under shear.[12−15] The β-form exhibits improved elongation at break and excellent impact strength,[16−18] especially at low temperatures, which can be attributed to the β−α polymorphous transition and the loose structure in β-crystals (compared with α-crystals) that are in favor of absorbing impact energy.[7a,14] The other two modifications in iPP are relatively rare.[19−21]

The α-crystals with inferior toughness are usually present in industrial products prepared by conventional processing techniques. Toughening of iPP has thus become an important research subject.[22] Up to now, four approaches have been proposed to improve the toughness of iPP, including copolymerization with other olefin monomers,[23] blending with rubber or thermoplastic elastomer,[24] compounding with organic or inorganic fillers (e.g., nanoparticles),[25,26] and addition of β-nucleating agent.[5−9] Compared with other approaches, the method of adding β-nucleating agent can induce high concentration of β-crystals and thus has some additional advantages, such as addition of very low nucleator content, little influence on the processing properties of iPP, and high performance/cost ratio, making itself a popular way to improve the toughness of iPP. The β-nucleating agent can induce a large amount of β-crystals through strong heterogeneous nucleation and enhanced epitaxial growth of β-crystals.[27,28] Generally speaking, the content of β-nucleating agent,[29,30] the molecular weight of iPP,[30,31] and the final temperature of heating[32−34] can all affect the activity of β-nucleating agent and in turn the content and morphology of β-crystals.

Concerning the formation of β-crystals, shear flow also plays an important role. In 1973, Leugering first observed that the shear flow could initiate the formation of β-crystals.[12] Subsequently, thermo-optical observation made by Varga et al.[14] showed that shear, caused by fiber pulling, was related to the development of α-row nuclei. The surface of the α-row nuclei could induce β-crystals, resulting in a cylindritic structure with polymorphic composition. Hsiao et al.[15] further used in-situ synchrotron wide-angle X-ray diffraction (WAXD) to investigate the shear-induced crystallization in iPP. They observed the formation of oriented α-crystals occurred immediately after application of shear flow, and subsequently β-crystals grew on the surface of the oriented α-crystals. The content of β-crystals was dependent on the amount of surface area of oriented α-crystals generated at different shear rates. It was also evidenced by means of in-situ optical microscopy that even at a low shear

*To whom correspondence should be addressed. E-mail: zmli@scu.edu.cn (Z.-M.L.), bhsiao@notes.cc.sunysb.edu (B.S.H.).

 Published on Web 07/28/2010

rate the β-spherulites still could be originated from the oriented α-crystal fronts.[35] It is natural to assume that under shear flow the β-nucleated iPP melt could form a higher fraction β-crystals. In other words, the combination of shear flow and β-nucleating agent should synergistically induce more β-crystals. Surprisingly, Varga et al.[36] first found that the high shear rate in fact restrained the formation of β-crystals. Huo et al.[37] performed a systematic study on crystallization of β-nucleated iPP and observed that as the shear rate increased, the content of β crystals consistently decreased, showing a counteraction effect between the shear flow and β-nucleating agent for the formation of β-crystals.

This counteraction does not necessarily represent any setback to simultaneously enhance strength and toughness of iPP. Using the combined effects of shear flow and β-nucleating agent, we have successfully fabricated iPP samples with considerably improved strength and toughness using an industrial injection molding machine.[38] Upon formation of the outer layer of the sample, an intense shear flow was applied, which induced highly oriented α-crystals in shish-kebab form (the process suppressed the formation of β-crystals) for improved strength, while the formation of the core layer occurred under static conditions, producing high concentration of β-crystals for improved toughness. Our finding suggests that with the suitable combination of shear flow and β-nucleating agent some synergy can be achieved by industrial processing. However, in order to manipulate the structure and property of iPP in a most effective manner, it is necessary to reveal the mechanism of this counteraction in situ. The questions that need to be addressed are as follows. (1) When shear flow and β-nucleating agent coexist, which crystal nucleates first, α- or β-crystals? (2) Which is the dominant step for the suppression of β-crystals, the nucleation or growth stage? (3) What are the contributions from the shear-induced homogeneous nuclei and β-nucleator-induced heterogeneous nuclei in the total nuclei? (4) How does the fraction of α- and β-crystals develop when β-nucleated iPP isothermally crystallizes under different shear rates? The answers to these questions shall allow us to obtain a relatively comprehensive understanding of the underlying mechanism.

In the present work, nucleation and growth processes of α- and β-crystals in β-nucleated iPP under shear flow were characterized by in-situ synchrotron wide-angle X-ray diffraction (WAXD) and small-angle X-ray scattering (SAXS) techniques. It was observed that when shear was applied to the β-nucleated iPP melt, the higher shear rate, the fewer β-crystals. The reduction of β-crystals was not because shear destroyed the structure of β-nucleating agent, or the oriented α-row nuclei induced by shear went against the formation of β-crystals, but because the amount of α-nuclei induced by shear and interactions between shear and β-nucleating agent was in the same order of magnitude as that of β-nuclei induced by β-nucleating agent in the nucleation process. During the growth process, α- and β-crystals grew competitively, resulting in the increase of α-crystals but decrease of β-crystals. Moreover, as the shear rate increased, more α-nuclei were formed, causing less β-crystals left. However, β-crystals were still prevailing in sheared, β-nucleated iPP.

Experimental Section

Materials. The iPP sample (model T30S) was purchased from Dushanzi Petroleum Chemical Co., China, with a melt flow rate (MFR) of 3 g/10 min (230 °C, 21.6 N), $M_w = 39.9 \times 10^4$ g mol^{-1}, and $M_w/M_n = 4.6$. The β-nucleating agent was aryl amide compounds (TMB-5), which had a similar chemical structure as some aromatic amine β-phase NA, such as *N,N′*-dicyclohexyl-2,6-naphthalenedicarboxamide.[33,34] This compound was supplied by Fine Chemical Institute, Shanxi, China.

Preparation of β-Nucleated iPP. TMB-5 was first melt mixed with iPP in a twin-screw extruder to form a master batch containing 1.0 wt % β-nucleating agent. The master batch was further melt compounded with pure iPP to produce pellet samples having 0.2 wt % of TMB-5. The screw speed was fixed at 82 rpm, and the processing temperature profile was limited within 170−180 °C from hopper to die. The pure iPP pellets without nucleating agents were also prepared under the same processing conditions for comparison purposes. For convenience, iPP with 0.2 wt % β-nucleating agent was designated as iPP02 while pure iPP as iPP0.

X-ray Measurements. WAXD and SAXS measurements were carried out at the Advanced Polymers Beamline (X27C, λ = 0.1371 nm) in the National Synchrotron Light Source (NSLS), Brookhaven National Laboratory (BNL). A MAR CCD X-ray detector (MARUSA) was employed for detection of 2D-WXAD and 2D-SAXS images, having a resolution of 1024 × 1024 pixels (pixel size = 158.44 μm). The data acquisition time was 20 s for each scattering pattern (image). The sample-to-detector distance was 112.6 and 2330 mm for WAXD (calibrated by an aluminum oxide (Al_2O_3) standard) and SAXS (calibrated by a silver behenate (AgBe) standard), respectively. The scattered intensities were registered in the range of scattering angles 2θ from 0 to 30°.

Linear WAXD and SAXS profiles were obtained from circular integration of intensities from 2D-WAXD and 2D-SAXS images, respectively. The intensity was plotted as a function of the scattering vector, q, where $|q| = 4\pi \sin\theta/\lambda$, with λ being the wavelength of the incident beam and 2θ being the scattering angle. Subsequently, through deconvoluting the peaks in linear WAXD profiles, the overall crystallinity X_c was calculated by

$$X_c = \frac{\sum A_{cryst}}{\sum A_{cryst} + \sum A_{amorp}} \quad (1)$$

where A_{cryst} and A_{amorp} are the fitted areas of crystal and amorphous peaks, respectively. The relative amount of the β-crystals K_β was evaluated by the method of Turner Jones et al.[39] and modified by Hsiao et al.[15,37]

$$K_\beta = \frac{A_\beta(300)}{A_\beta(300) + A_\alpha(110) + A_\alpha(040) + A_\alpha(130)} \quad (2)$$

A_β (300) is the area of the (300) reflection peak; A_α (110), A_α (040), and A_α (130) are the areas of the (110), (040), and (130) reflection peaks, respectively. Meanwhile, the crystallinity of β-crystals (X_β) and the crystallinity of α-crystals (X_α) are given by

$$X_\beta = K_\beta X_c \quad (3)$$

$$X_\alpha = X_c - X_\beta \quad (4)$$

For convenience, the absolute crystallinity of α- and β-crystals was designated as X_c^α and X_c^β, respectively, while the relative crystallinity of α- and β-crystals was designated as X_r^α and X_r^β, respectively. As for linear SAXS data, the crystalline lamellar long period (L_B) was defined as $L_B = 2\pi/q$.

Experimental Procedures. A Linkam CSS-450 high-temperature shearing stage modified for in-situ X-ray scattering studies was used to precisely control the shear flow and thermal history of the polymer samples. The temperature protocol and shear conditions used during the WAXD and SAXS measurements are shown in Figure 1. The experimental temperature profiles were set as follows: (1) heating at a rate of 30 °C/min from room temperature to 210 °C; (2) holding the temperature at 210 °C for 300 s to eliminate residual structure; (3) cooling at a rate of 30 °C/min down to 134 °C; (4) holding the temperature at 134 °C for at least 900 s for X-ray measurements.

Results

Two-Dimensional Wide-Angle X-ray Diffraction Patterns. A representative series of 2D-WAXD images of isothermally

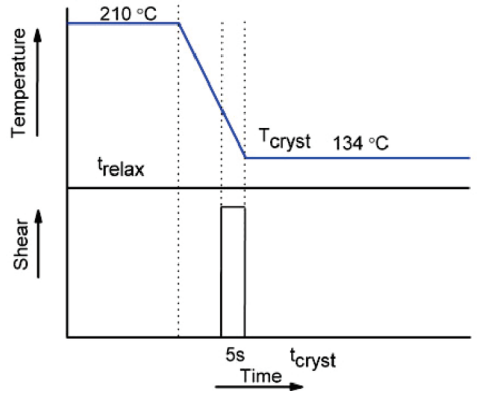

Figure 1. Schematic diagram of the temperature and shear conditions as a function of time during step shear in WAXD and SAXS experiments.

crystallized iPP0 and iPP02 samples at 134 °C with and without shear flow (0, 15, 30 s^{-1}) are shown in Figure 2. Figures 2a1−2a4 represent the iPP0 sample crystallized under quiescent conditions. The characteristic lattice planes of α-crystals, i.e., (110), (040), (130), (111), and (−131), from inner to outer, were found to develop homogeneously (Figures 2a1−2a3) until the completion of crystallization (Figure 2a4), without the appearance of β-crystals. When a shear flow was applied to iPP, the samples showed similar growth features (Figures 2b,c) despite different shear rates (15 and 30 s^{-1}) used. The initial images (Figures 2b1 and 2c1) exhibited a diffuse scattering pattern. Even though the melt might possess orientation, which could not be determined due to the detection limitation of the WAXD technique. However, after 40 s, sharp α-crystal lattice planes (040) and (110) were clearly observed, which exhibited the arclike diffraction feature from oriented α-crystals (Figures 2b2 and 2c2). Subsequently, arclike (300) reflection from β-crystals was further identified at t = 60 s (Figures 2b3 and 2c3), indicating the inception of oriented β-crystals. The diffraction intensities of both α- and β-crystals became stronger with time due to the growth of crystallites. After a certain time, the diffraction intensities of all crystal reflections remained constant, indicative of completion of crystallization (Figures 2b4 and 2c4). It is interesting to note that the (300) reflection of β-crystals remained isotropic, which could be attributed to the spontaneous growth of β-crystals without any preferential orientation,[15] whereas α-crystals persisted some orientation, and the degree of orientation decreased with time due to the spatial growth of crystallites with less preferred orientation.

For iPP02 sample under quiescent isothermal conditions (Figure 2d), both (300) and (131) reflections from β-crystals increased notably (the diffraction intensities became visible at t = 20 s, as seen in Figure 2d2) due to the strong nucleating effect of β-nucleating agent. The growth of β-crystals was intense throughout the entire crystallization process (Figures 2d3 and 2d4), but the crystallites formed were unoriented β-crystals. Upon application of shear, an interesting phenomenon was observed. That is although the initial crystals were unoriented β-crystals (Figure 2f1), the subsequently formed crystals included oriented α-crystals with enhancing (040) reflection as well as unoriented β-crystals with enhancing (300) reflection (Figures 2e2 and 2f2). The diffraction intensities of both α- and β-crystals became stronger with time due to the growth of the crystallites (Figures 2e3 and 2f3). However, the resulting β-crystals possessed no orientation; only α-crystals were partially oriented. The orientation decreased with time because of the spatial growth of α-crystals.

The above results are different from the earlier observation by Hsiao et al.[15] that oriented α-crystals are responsible for the growth of β-crystals in pure iPP melts. In other words, the shear flow induces the oriented α-row-nuclei first and then β-crystals grow on the surfaces of the oriented α-crystals. In this study, it was seen that when shear was applied to β-nucleated iPP, unoriented β-crystals developed first, and oriented α-crystals appeared subsequently. This phenomenon has not been reported in the literature before. The initial β-crystals could be attributed to the β-nucleating agent, whereas the application of shear induced oriented α-row-nuclei and subsequent growth of oriented α-crystals (Figures 2e2 and 2f2). It was seen that crystallites appeared at t = 20 s in Figures 2b−2f, indicating that shear, β-nucleating agent, or the combined effects could all accelerate the crystallization of iPP. However, it is difficult to distinguish which factor, shear or β-nucleating agent, has a more pronounced effect on the acceleration of crystallization.

Analysis of Linear Wide-Angle X-ray Diffraction Profiles. In order to further understand the development of different crystals as a function of time, linear WAXD profiles were analyzed (results shown in Figure 3). Figures 3a and 3d show the crystal growth of iPP0 and iPP02 under quiescent conditions. In iPP0, only α-crystals developed with time without the appearance of β-crystals. In iPP02, β-crystals prevailed due to the addition of β-nucleating agent, which has been reported by several research groups.[40,41] In iPP0, it was seen that α-crystals induced by shear (shear rate = 15, 30 s^{-1}) took place at t = 20 s (i.e., the second curve in Figures 3b and 3c), while β-crystals, probably originated from α-crystals, appeared at t = 40 s with a distinct time lag.[15] In contrast, in iPP02 under shear, β-crystals (induced by β-nucleating agent) appeared first at t = 20 s; subsequently, α-crystals induced by shear appeared at t = 40 s (Figures 3e and 3f), showing a different growth process when compared to iPP0 under shear. Under shear, β-nucleating agent, or the combined effects, the growth rates of both crystals were accelerated.

To determine the evolution of β-crystals, β-phase crystallinity (X_c^β) and its relative crystallinity (X_r^β) as a function of crystallization time are present in Figures 4 and 5, respectively. The quiescently, isothermally crystallized iPP0 showed no β-crystals as observed from Figures 4a and 5a. With application of shear (15 s^{-1}), β-crystals appeared and their content increased with the crystallization time (Figures 4b and 5b), until it reached a plateau at about t = 140 s where X_c^β = 0.082 and X_r^β = 20.4% (Table 1b). As the shear rate increased to 30 s^{-1} (Figures 4c and 5c), the content of β-crystals increased to X_c^β = 0.096 and X_r^β = 21.7% (Table 1c), while the corresponding saturation time was shortened to around 120 s. It was apparent that the content of β-crystals in iPP0 increased with the shear rate. From Figures 5b and 5c, one could conclude that when the crystallization started, the initial contribution of β-crystals to the overall crystallinity was 0 while the α-crystals occupied 100% (Figures 7b and 7c), which again confirmed that the shear flow was responsible for the induction of α-crystals.

In iPP02 (Figures 4d and 5d), β-nucleating agent provided a large amount of heterogeneous nucleation sites for the growth of β-crystals. As a result, the content of β-crystals could achieve saturation at about 100 s. The final crystallinity was mainly from β-crystals with X_c^β = 0.480 and X_r^β = 91.4% (Table 1d). However, when shear (15 s^{-1}) was applied (Figures 4e and 5e), the content of β-crystals decreased to X_c^β = 0.400 and X_r^β = 70.2% (Table 1e). As the shear rate

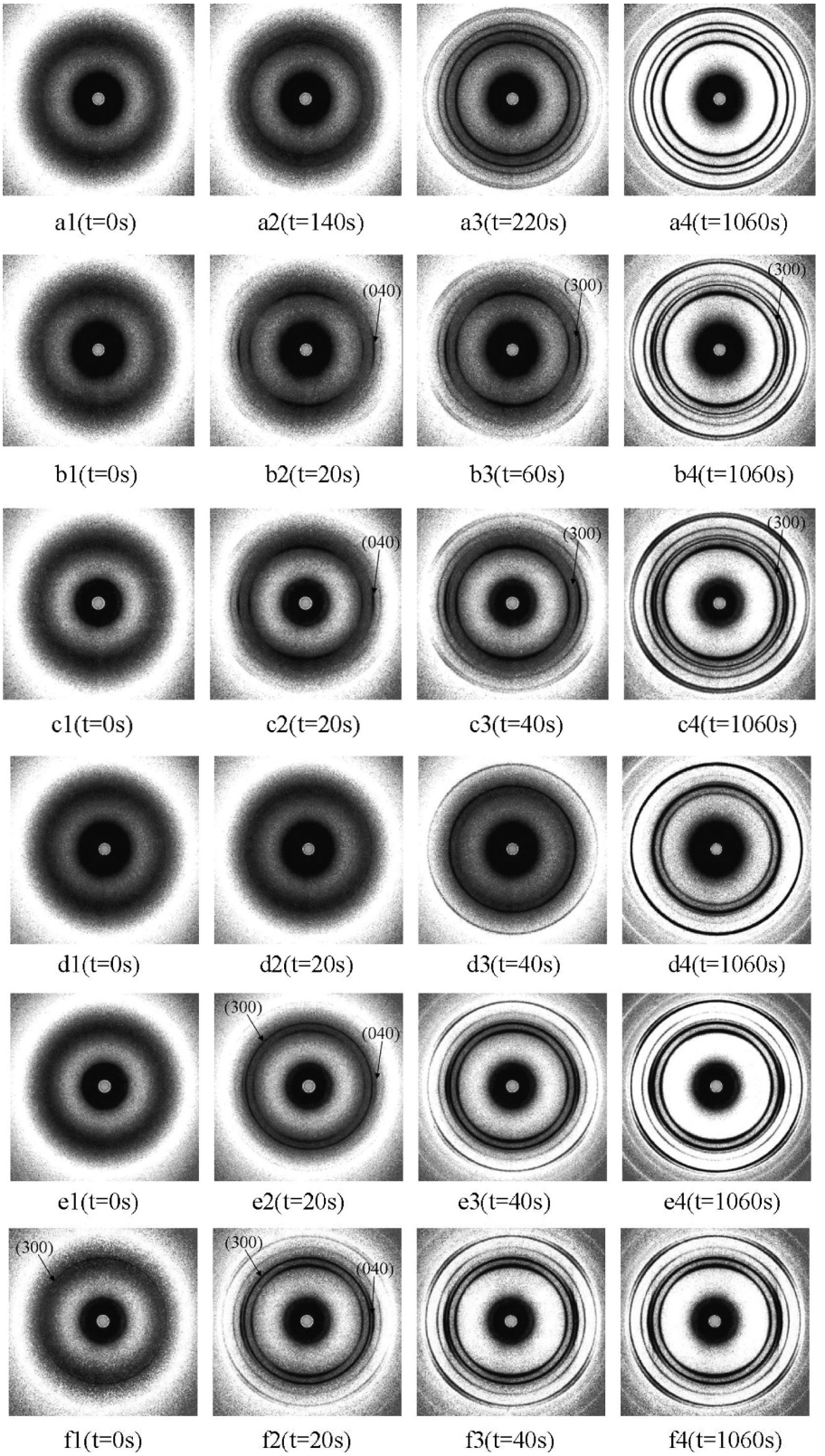

Figure 2. Selected 2D-WXAD patterns, showing the crystal growth of iPP isothermally crystallized at 134 °C: (a) iPP0 without shear, (b) iPP0 at a shear rate of 15 s^{-1}, (c) iPP0 at a shear rate of 30 s^{-1}, (d) iPP02 without shear, (e) iPP02 at a shear rate of 15 s^{-1}, and (f) iPP02 at a shear rate of 30 s^{-1}.

further increased to 30 s^{-1} (Figures 4f and 5f), a greater reduction of the β-crystal content was observed, i.e., $X_c^\beta = 0.300$ and $X_r^\beta = 59.0\%$ (Table 1f), and the saturation time was shortened to 60 s. In Figures 5e and 5f, the initially relative crystallinity of β-crystals in iPP02 was 100%, whereas the corresponding relative crystallinity of α-crystals was equal to 0 (Figures 7e and 7f), implying that the initially formed crystallites were mainly induced by the β-nucleating agent even under the shear flow. The subsequent reduction of the β-crystal fraction resulted from the rapid increase of α-crystals induced by shear. As time went on, the relative crystallinity of β-crystals increased again, which could be attributed to the

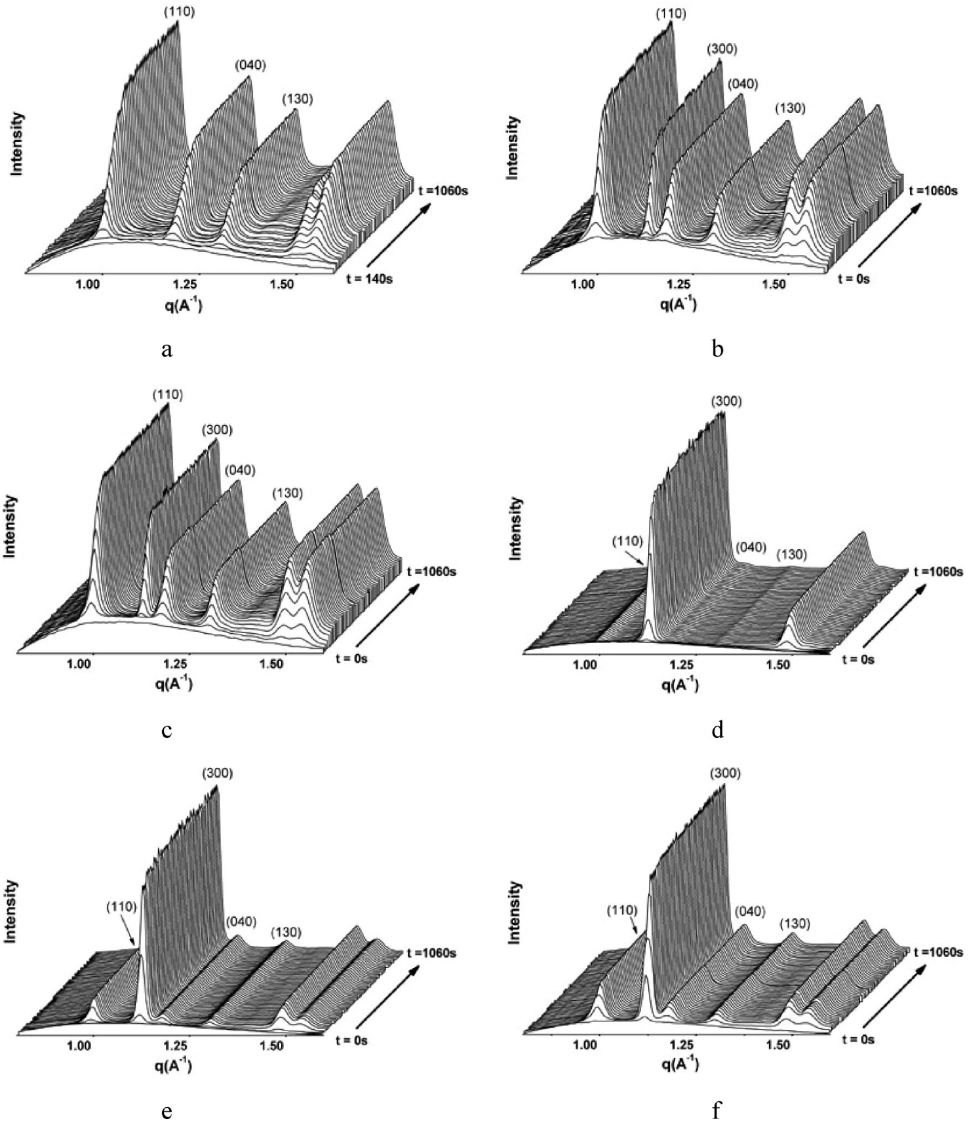

Figure 3. Linear WAXD intensity profiles as a function of scattering sector, q, of iPP melt, obtained from circularly integrated intensities of 2D-WAXD patterns in Figure 2. The conditions of a−f are the same as Figure 2.

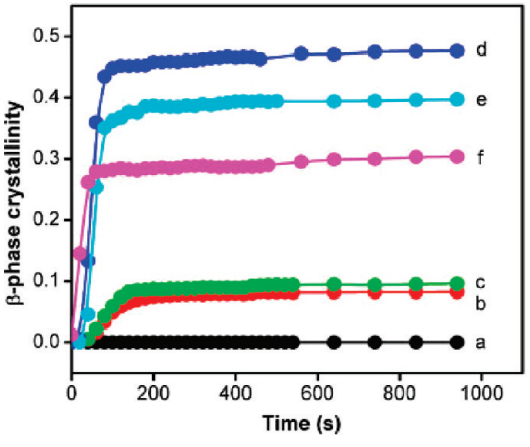

Figure 4. The β-phase crystallinity in the iPP melt as a function of crystallization time, obtained from their linear WAXD in Figure 3. The conditions of a−f are the same as Figure 2.

effect of β-nucleating agent or epitaxial growth of β-crystals on existing α-crystals. The content of β-crystals in iPP02 decreased by the application of shear (Figure 4e)

Table 1. β-Phase Crystallinity (X_c^β), Relative Crystallinity (X_r^β), and Half-Time of β Crystallization at 134 °C

	β-phase crystallinity	relative crystallinity (%)	half-time of β crystallization (s)
a	0	0	
b	0.082	20.4	88.8
c	0.096	21.7	87.1
d	0.480	91.4	49.8
e	0.400	70.2	55.7
f	0.300	59.0	19.9

and the increase of shear rate (Figure 4f). The reason for depression of β-crystals in β-nucleated iPP sample under shear will be discussed further.

For comparison, α-phase crystallinity (X_c^α) and relative crystallinity (X_r^α) of α-crystals are also shown in Figures 6 and 7. Basically, the content of α-crystals underwent an opposite evolution process of β-crystals. However, it is noteworthy that, when the crystallinity of β-crystals increased with the shear rate (Figures 4b and 4c), the crystallinity of α-crystals in iPP0 at shear rate = 30 s^{-1} (Figure 6c) did not decrease but increased. This result indicates that the increase of β-crystals was not at the expense of α-crystals.

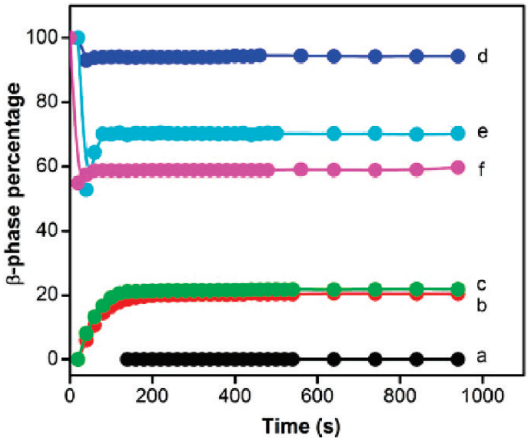

Figure 5. Relative crystallinity of β-crystals (ratio of individual crystallinity to the overall crystallinity) as a function of crystallization time, obtained from their linear WAXD in Figure 3. The conditions of a−f are the same as Figure 2.

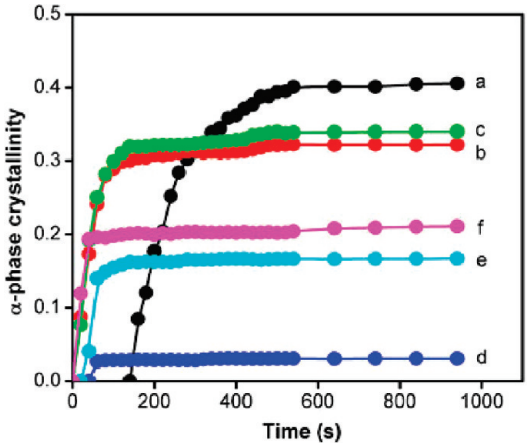

Figure 6. The α-phase crystallinity in the iPP melt as a function of crystallization time, obtained from their linear WAXD in Figure 3. The conditions of a−f are the same as Figure 2.

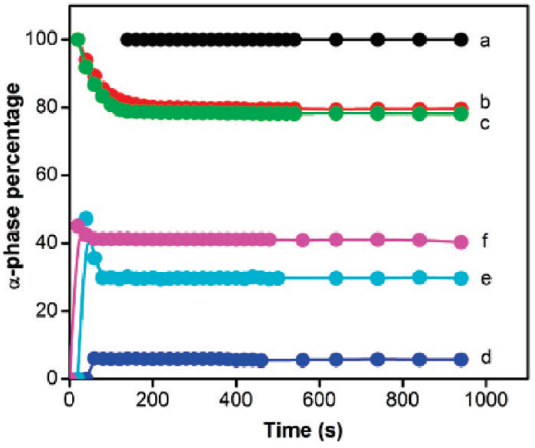

Figure 7. Relative crystallinity of α-crystals (ratio of individual crystallinity to the overall crystallinity) as a function of crystallization time, obtained from their linear WAXD in Figure 3. The conditions of a−f are the same as Figure 2.

Small-Angle X-ray Scattering. Different lamellar arrangements (e.g., stacking manners) in α- and β-crystals could be detected by SAXS measurement. Selected 2D-SAXS patterns obtained when isothermal crystallization at 134 °C was finished are illustrated in Figure 8. iPP0 showed isotropic scattering under quiescent crystallization (Figure 8a), while iPP02 indicated intense scattering along the equator due to strongly anisotropic epitaxial growth of iPP by β-nucleating agent (Figure 8d).[32,33] As for the sheared melt of iPP0 and iPP02, the strong scattering maxima on the meridian are clearly seen in Figures 8b, 8c, and 8f, resulting from the lamellae growth perpendicularly to the shear direction.

The linear SAXS profiles and the corresponding long periods (L_B) evolution as a function of crystallization time are illustrated in Figures 9 and 10, respectively. It is well documented that α-crystals have a monoclinic unit cell with a = 0.665 nm, b = 2.096 nm, and c = 0.650 nm,[3,42] while β-crystals have a trigonal unit cell with $a = b$ = 1.103 nm and c = 0.649 nm.[43] All the long periods started from a maximum value, then decreased continuously, and reached an equilibrium value (Figure 10). The decrease was associated with the progression of crystallization, resulting in the reduction of average long periods. For iPP0 sample crystallized at 134 °C (Figure 10a), α-crystals occupied 100% of the crystallites, having the shortest L_B = 19.52 nm among all the samples. As for iPP02 crystallized at 134 °C (Figure 10d) having the β-crystal content of 91.4%, L_B (25.38 nm) was the longest. The above results could be attributed to the different stacking manners in α- and β-crystals. The α-crystals of iPP consisted of a cross-hatched structure of parent and daughter lamellae, where the daughter lamellae nucleated and grew from the previously formed primary lamellae (the parent lamellae).[28,44] As a result, the long period of α-crystals was small. As for β-crystals, it was reported that the growth of β-crystals proceeded mainly by branching around screw dislocations, resulting in new lamellae that often diverged from the initial lamellar arrangement.[45] When iPP0 was subjected to shear (Figures 10b and 10c), the long periods of both samples increased to 22.06 and 21.48 nm, respectively. It has been reported that the average long period from oriented crystallites is generally larger than that of the unoriented crystallites.[46] Thereby, the increase of long period can be ascribed to the formation of oriented crystallites (Figures 8b and 8c) and β-crystals (Tables 1b and 1c). A dramatic reduction of the long period happened in the sheared, β-nucleated iPP sample (Figure 10f), which was shortened to 20.04 nm, almost equaling that of the quiescent iPP0 sample (Figure 10a).

Discussion

It has been well established that shear flow can accelerate the crystallization process of semicrystalline polymers and induce some unique crystalline morphology such as shish-kebabs that can profoundly affect the properties of shaped products.[39,47,48] Therefore, the behavior of shear-induced crystallization has been an active research area.[49−54] The application of shear can also trigger different polymorphism in iPP, such as β-crystals with desired properties of high toughness and elongation at break. But how does shear induce the formation of β-crystals in iPP? One possible scenario is that shear flow causes the development of α-row nuclei, and the surface of the α-row nuclei induces the growth of β-crystals in iPP.[14,15]

The β-nucleating agent can induce a high proportion of β-crystals due to strong heterogeneous nucleation.[27,28] It is reasonable to argue that when shear was applied to β-nucleated iPP, more β-crystals would be formed. However, it has been found that the introduction of shear in fact decreased the content of β-crystals in β-nucleated iPP. Furthermore, the higher the shear rate applied, the less content of β-crystals formed. In this study, we used in-situ synchrotron WAXD and SAXS to follow the nucleation and growth processes of α- and β-crystals and obtain information that

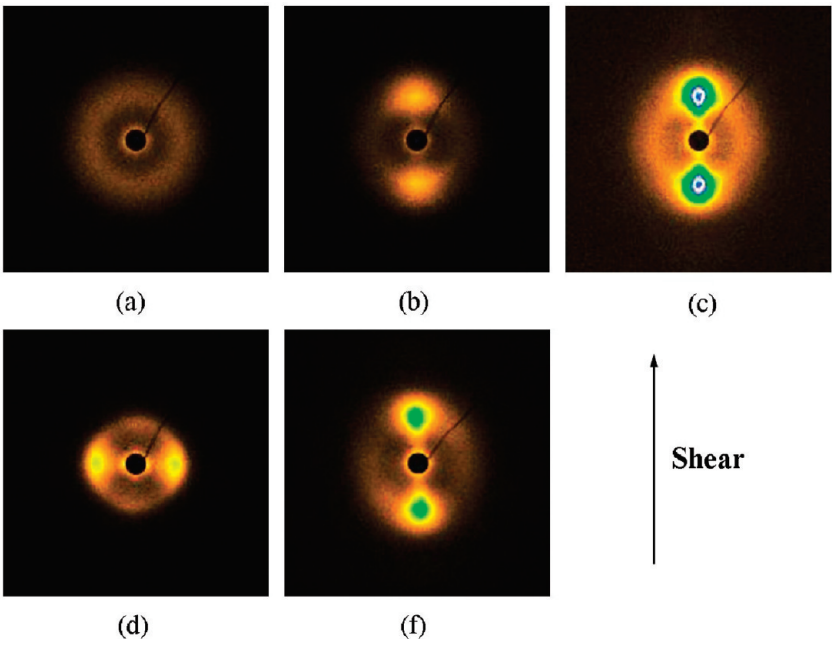

Figure 8. 2D-SAXS patterns of complete crystallization at 134 °C. The conditions of a−f are the same as Figure 2.

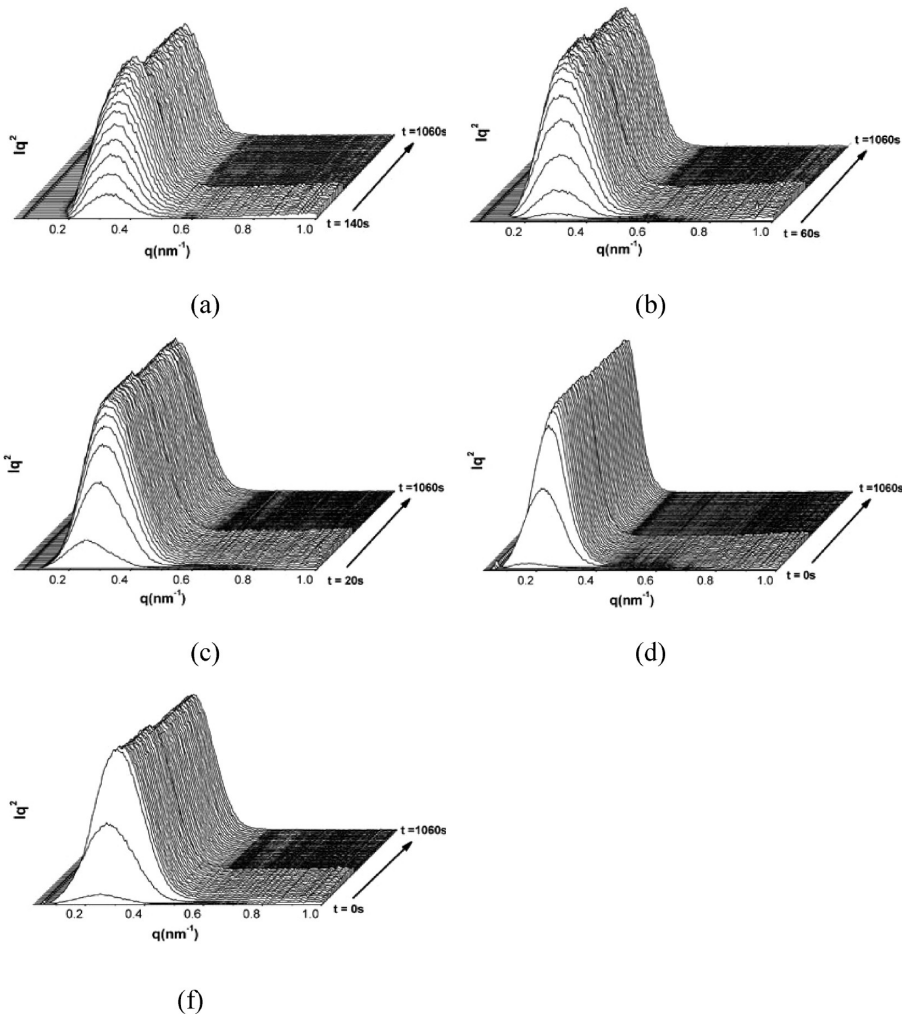

Figure 9. Linear SAXS intensity profiles as a function of scattering sector, q, of iPP melt, obtained from circularly integrated intensities of 2D-SAXS patterns in Figure 8. The conditions of a−f are the same as Figure 2.

is helpful to understand the phenomenon of β-crystal depression in β-nucleated iPP sample under shear flow.

Naturally, it is easy to consider that shear may destroy the structure of β-nucleating agent, causing it to lose the effectiveness. To verify this, we reheated the already shear crystallized iPP02 sample (30 s^{-1}) to 210 °C, held at this temperature for 300 s to erase the history of the first crystallization, and then cooled to 134 at 30 °C/min to quiescently crystallize. The in-situ 2D-WAXD and corresponding linear WAXD patterns are shown in Figures 11 and 12, respectively. It is clearly shown that β-crystals emerged quickly at t = 0 s (Figure 11g1), mainly in β-crystals. The crystals grew rapidly, such that at t = 160 s the content of β-crystals already reached a plateau value (X_c^β = 0.500), being close to 0.480, the β-phase crystallinity of iPP02 sample obtained from direct isothermal crystallization at 134 °C (Table 1d). Therefore, it can be logically concluded that the reason for the decreased β-crystals in sheared, β-nucleated iPP was not due to the damage of the structure of β-nucleating agent.

From the conventional point of view, crystallization is a two-step process: (1) formation of stable nuclei (i.e., the nucleation stage) followed by (2) crystal growth characterized by the crystal growth rate (G).[55,56] At a given pressure (that is atmospheric pressure in the present case), G is set by the temperature. As crystallization is performed under isothermal conditions, the linear growth rate of a certain crystal form is fixed. Hence, the observed macroscopic variations in relative amounts of α- and β-crystals are definitely ascribed to variations of α- and β-nuclei in the nucleation stage and growth rate of α- and β-crystals in the growth step.

For isothermal crystallization at T_c, the following contributions to nucleation density (number of nucleation sites per unit volume, i.e., nuclei/m^3) should be considered. (1) $N_{hom}(T_c,t)$: homogeneous nuclei generated in the system by thermally activated local density fluctuations. In many practical situations, the contribution is small and can be disregarded, especially for short crystallization time.[57] (2) $N_{het}^0(T_c)$: unavoidable nuclei from impurities. (3) $N_{het}^A(T_c)$: heterogeneous nuclei originated from the addition of nucleating substances. (4) In the case of application of shear, $N_s(T_c,T_s,t_s,\gamma,M)$: shear-induced nuclei can be regarded as homogeneous nuclei due to the direct effect of shear on the polymer itself. (5) ΔN_s^A: nuclei arose from the interactions between shear flow and the nucleating agent.[57]

To be more concise, the sources of α- and β-crystals are briefly described in Figure 13. In quiescent crystallization of iPP0 (Figure 2a) at T_c, $N_{hom}(T_c,t)$ and $N_{het}^0(T_c)$ are the main α-nuclei for α-crystal growth. In the case of isothermal crystallization of sheared iPP0 (Figures 2b and 2c) at T_c in a short crystallization time ($\tau_{1/10}$), N_s is the dominant source for α-nuclei in the nucleation stage, which is responsible for α-crystal growth. While in quiescent crystallization of iPP02 (Figure 2d) at T_c, abundant $N_{het}^A(T_c)$ provides the β-nucleation sites for β-crystal growth. When shear is applied or β-nucleating agent is added to the samples, $N_{het}^0(T_c)$ and $N_{hom}(T_c,t)$ can be ignored. When the shear is applied to iPP02 (Figures 2e and 2f), N_s and N_{het}^A coexist; in the

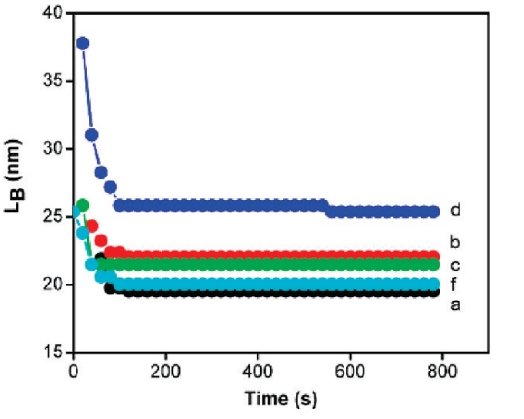

Figure 10. Time evolution profiles of the long periods as a function of crystallization time. The conditions of a−f are the same as Figure 2.

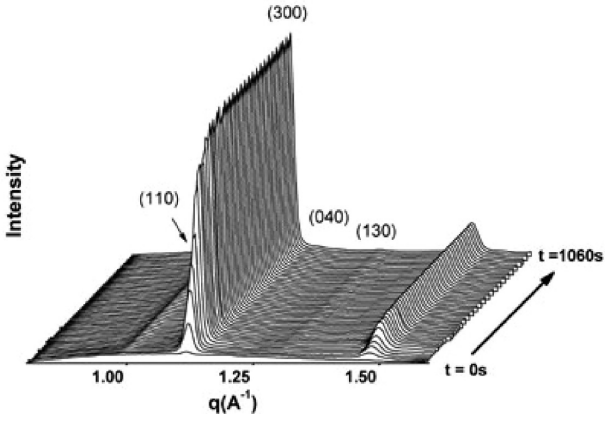

Figure 12. Linear WAXD intensity profiles as a function of scattering sector, q, of iPP02 melt, obtained from circularly integrated intensities of 2D-WAXD patterns in Figure 11.

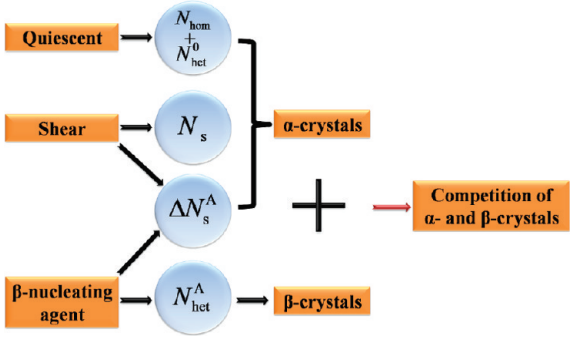

Figure 13. Brief description of the sources of α- and β-crystals and the competition of α- and β-crystals.

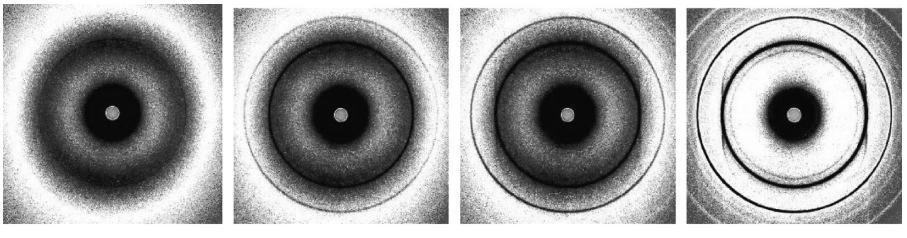

Figure 11. Selected 2D-WXAD patterns showing the crystal growth process of iPP02 isothermally crystallized at 134 °C, after heating sample to 210 °C for 300 s and then decreasing to 134 °C.

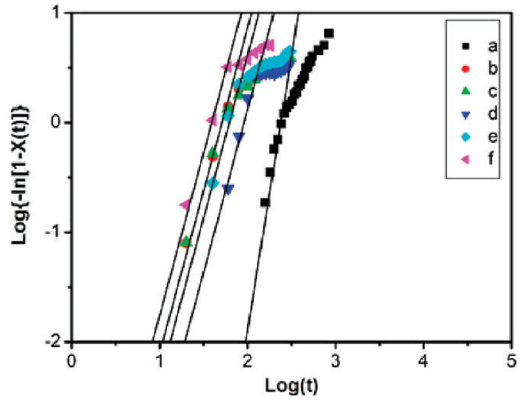

Figure 14. Avrami plots of the crystallization data for α-crystals. The conditions of a−f are the same as Figure 2.

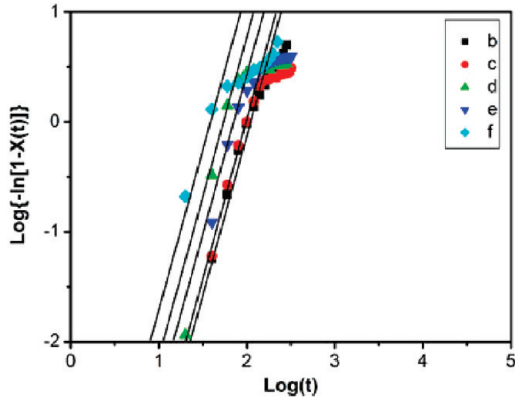

Figure 15. Avrami plots of the crystallization data for *β*-crystals. The conditions of b−f are the same as Figure 2.

meantime, ΔN_s^A arises and can be believed to provide α-nuclei because interactions between shear and *β*-nucleating agent can greatly lower the entropy of the system, which favors the formation of α-nuclei, compared to the sole application of shear.

After cessation of a mild shear or addition of *β*-nucleating agent in a short crystallization time (e.g., $t = \tau_{1/10}$), the nucleation sites can be assumed to be in the regime of pointlike nucleation.[58] In order to reveal the growth geometry of α- and *β*-crystals, the Avrami equation was adopted.

$$X(t) = 1 - \exp(-kt^n) \tag{5}$$

Rewriting eq 5 in the following form:

$$\log\{-\ln[1 - X(t)]\} = n\log(t) + \log(k) \tag{6}$$

where k is the bulk crystallization constant and n is the Avrami exponent.

Figures 14 and 15 show that the Avrami exponent n (the slope of curves) of α- and *β*-crystals is constantly equal to 3, except for the quiescent crystallization of pure iPP, which is equal to 4. The divergence of the curves may be ascribed to slow secondary crystallization. Herein, the growth of α- and *β*-crystals can be described by the spherulite model in the process of crystallization.

The nucleation density N can be extracted from the progress of crystallinity using the Kolmogoroff−Avrami−Evans equation:[59,60]

$$X(t) = 1 - \exp\left(-\frac{4\pi}{3}NG^3t^3\right) \tag{7}$$

Table 2. Experimentally Determined Number of Nuclei per Cubic Meter at $X = 0.1$[a]

	$\tau_{1/10}$ (s)	$N_{hom}(T_c,t) + N^0_{het}(T_c)$	N_s	N^A_{het}	$N^A_{het} + N_s + \Delta N^A_s$
a	150.0	1.2×10^{14}			
b	21.6		4.0×10^{16}		
c	19.1		5.7×10^{16}		
d	17.4			5.5×10^{16}	
e	13.2				15×10^{16}
f	10.5				29×10^{16}

[a] The conditions of a−f are the same as Figure 2.

The nucleation density can be estimated by rewriting eq 7 in the following form:

$$N = -\frac{3}{4\pi G^3}\frac{\ln(1 - X)}{t^3} \tag{8}$$

where $X = 0.1$ and $t = \tau_{1/10}$ in order to reduce the interference between the growing crystallites and the effect of $N_{hom}(T_c,t)$. The growth rate of α-spherulites $G_\alpha = 2.39\ \mu$m min^{-1} = 3.98×10^{-8} m s^{-1} (T_c = 134 °C)[61] can be used in the cases of Figures 2a−2c, while the growth rate of *β*-spherulites $G_\beta = 2.65\ \mu$m min^{-1} = 4.42×10^{-8} m s^{-1} (T_c = 134 °C)[61] can be used in the case of Figure 2d. The average value of G_α and G_β can be used in the cases of Figures 2e and 2f for approximate calculation. Therefore, all the nucleation density under the various experimental situations can be calculated, and results are listed in Table 2.

From the above results, it was clear that the nucleation density of iPP0 in quiescent crystallization (Table 2a) was 1.2×10^{14} nuclei/m^3, which was 2 orders of magnitude smaller than that of sheared iPP0 (Tables 2b and 2c) and iPP02 (Table 2d). When the shear flow (15 s^{-1}) was solely applied to iPP0 (Table 2b), N_s = 4.0×10^{16} nuclei/m^3, which represented the nucleation density of α-nuclei. While the shear rate increased to 30 s^{-1} (Table 2c), N_s rose up to 5.7×10^{16} nuclei/m^3. In the case of isothermal crystallization of iPP02 (Table 2d), N^A_{het} = 5.5×10^{16} nuclei/m^3, which was in the same order of magnitude of sheared iPP0. When the shear flow was applied to iPP02, shear-induced nuclei and ΔN_s^A (9.5×10^{16} nuclei/m^3, i.e., the last column in Table 2 minus N^A_{het}) for α-crystal growth and *β*-nucleator-induced nuclei for *β*-crystal growth (assumed to be 5.5×10^{16} nuclei/m^3) coexisted in iPP melt and were in the same order of magnitude; thus, competitive growth of α- and *β*-crystals occurred. The growth of α-nuclei-induced α-crystals naturally decreased the content of *β*-crystals in the limited growing space (Table 1e) compared to the quiescent isothermal crystallization of *β*-nucleated iPP (Table 1d). It was found that the α-nuclei (23.5×10^{16} nuclei/m^3) increased with the increase of shear flow, causing more reduction of *β*-crystals. Because of the favorable temperature (134 °C) for *β*-crystal growth, the growth of *β*-crystals was faster than that of α-crystals. In addition, the epitaxial growth of *β*-crystals on the existing α-crystals may occur.[61] As a result, *β*-crystals were still the dominant phase (Tables 1e and 1f), even though competitive growth of α-crystals also took place.

In order to verify the hypotheses that shear triggers α-nuclei for α-crystal growth and α- and *β*-crystals grow competitively, we performed another in-situ WAXD experiment whose temperature protocol and shear conditions are shown in Figure 16. iPP02 was first heated to 210 °C for 300 s to erase the thermal or mechanical history. Then the temperature decreased to 145 °C to quiescently crystallize for 300 s. After the crystalline diffractions were clearly observed, the sample was subjected to shear (shear rate = 30 s^{-1} and shear time = 5 s) and simultaneously cooled to 134 °C for isothermally crystallization until the crystallization was finished. The heating and cooling rates were both 30 °C/min. With regard to the results of this experiment, one of two cases can be supposed. One is that after the application of shear *β*-crystals

continued to grow, and its content was unaffected compared to the quiescently, isothermally crystallized iPP02. This would imply shear was not beneficial for the formation of α-nuclei. The other one is that after shear the sample exhibited the β-crystal content comparable to the directly sheared iPP02 (Table 1f). This case would suggest that shear induced abundant α-nuclei, which were favorable for α-crystal growth. As a result, β-crystal growth was restricted. The results of in-situ WAXD measurement are shown in Figures 17, 18, and 19.

Representative (300) lattice plane of β-crystals did not appear until $t = 80$ s (Figure 17h1), indicative of the slow growth rate as a result of higher crystallization temperature (145 °C). Every lattice plane of β-crystals grew homogeneously, while few α-crystals were observed as time went on (Figure 17h2). As soon as shear was applied to the melt, it was clearly observed that oriented (040) lattice plane of α-crystals emerged and diffraction intensity of α-crystals enhanced, while β-crystals remained unoriented and diffraction intensity seemed unchanged (Figure 17h3), implying that shear induced the formation of α-nuclei and accelerated the development of α-crystals even in the presence of β-nucleating agent. When the crystallization was finished, the diffraction intensity of α-crystals was enhanced greatly (Figure 17h4).

The corresponding linear WAXD profiles before ($t \leq 300$ s) and after shear ($t > 300$ s) are shown in Figure 18. After the application of shear, the development of α-crystals was greatly accelerated, as seen directly from the higher intensities for all reflection planes such as (110), (040), and (130) from α-crystals. In contrast, the intensity of the (300) reflection from β-crystals increased only slightly (the β-phase crystallinity as a function of crystallization time is shown in Figure 19h). For comparison, isothermal crystallization results from iPP02 at 134 °C (iPP02-134) and at 145 °C (iPP02-145) are also included in Figure 19. It was seen that the growth of β-crystals superposed the curve of iPP02-145 before 300 s due to their similar growth conditions. However, the content of β-crystals did not increase after shear ($t > 300$ s). Compared with results from iPP02-134 and iPP02-145, the final crystallinity of β-crystals in Figure 19h was only 0.310, lower than 0.400 from iPP02-145 and 0.480 from iPP02-134. As mentioned above, the decrease of β-crystals indicates that the shear-induced α-nuclei favored the α-crystal growth but restrained the β-crystal growth. The nucleation density of β-nuclei from iPP02 at 145 °C (before 300 s) should be smaller than that at 134 °C. This can be explained as follows. When the shear was introduced to iPP02, there were two phases in the melt: β-crystal solid phase and the melt phase. The interactions between melt and solid β-crystal phases would dramatically increase under shear flow, resulting in the increase of ΔN_s^A. As a result, more α-crystals were formed while the content of β-crystals remained nearly unchanged.

It was found that the amount of α-nuclei generated by shear flow as well as interactions between shear and β-nucleating agent

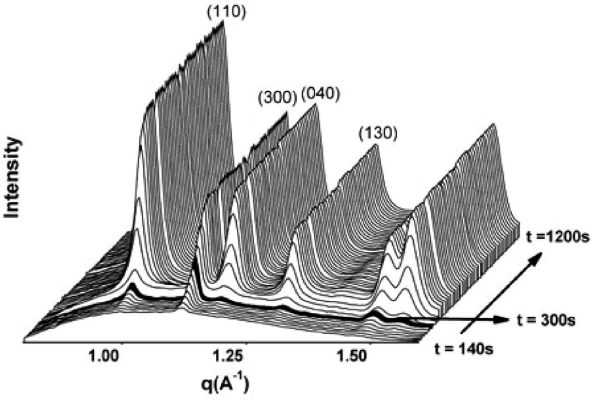

Figure 18. Linear WAXD intensity profiles as a function of scattering sector, q, of iPP melt, obtained from circularly integrated intensities of 2D-WAXD patterns in Figure 17.

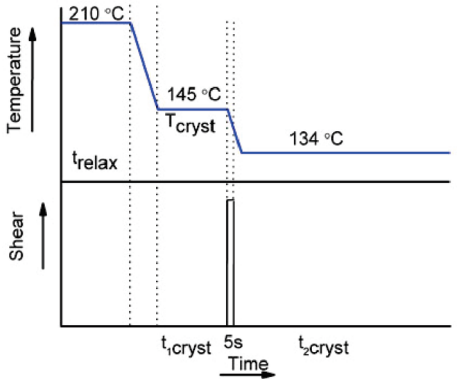

Figure 16. Schematic diagram of the temperature and shear conditions as a function of time during step shear in WAXD experiment.

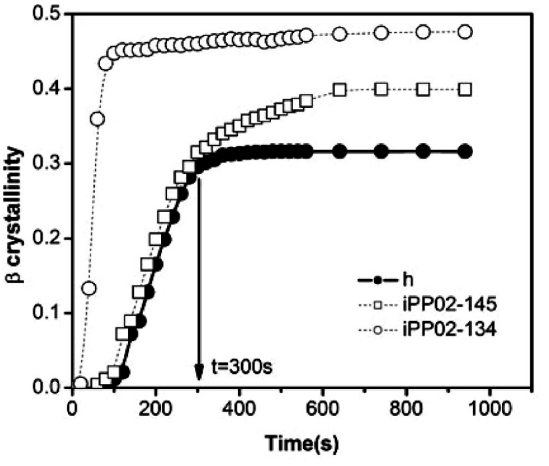

Figure 19. The β-phase crystallinity in the iPP melt as a function of crystallization time, obtained from its linear WAXD in Figure 18.

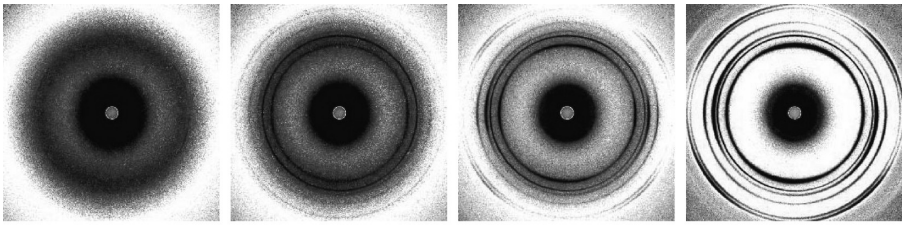

Figure 17. Selected 2D-WXAD patterns showing the crystal growth process of iPP02. First, iPP02 was isothermally crystallized at 145 °C for 300 s. Then, the shear was applied during cooling from 145 to 134 °C. Finally, iPP02 was isothermally crystallized at 134 °C.

was in the same order of magnitude as the amount of β-nuclei generated by β-nucleating agent, causing the competitive growth of α- and β-crystals afterward. This implies that the content of β-crystals would decrease due to the increase of α-crystals in the limited growing space. In the growth stage, the temperature is the key factor to influence the growth rate of α- and β-crystals. $T_c = 134$ °C favors the β-crystal growth and the epitaxial growth of β-crystals on the existing α-crystals.[61] That might be the reason why although the same order of magnitude of α- and β-nuclei was found in iPP melt at $T_c = 134$ °C, the final content of β-crystals was dominant (Tables 1e and 1f) after full crystallization. Thus, when the shear flow and β-nucleating agent coexisted, the depression of β-crystals compared to isothermal crystallization of iPP02 was expected because although the same order of magnitude of α- and β-nuclei formed in the nucleation stage, then α- and β-crystals competitively grew in the growth stage, leading to the increase of α-crystals but decrease of β-crystals. However, the temperature is favorable for β-crystal growth, so that the final content of β-crystals is still dominant.

Conclusions

The nucleation and growth processes of α- and β-crystals in the sheared iPP samples with and without β-nucleating agent were investigated by means of in-situ synchrotron WAXD and SAXS techniques. When shear was solely subjected to pure iPP melt, α-row-nuclei induced by shear were observed, resulting in the subsequent development of β-crystals, where the content of β-crystals increased with the shear rate. When both shear and β-nucleating agent coexisted, the formation of β-crystals emerged earlier than α-crystals due to the (heterogeneous) nucleating effect of β-nucleating agent and more favorable crystallization temperature for β-crystal growth. However, the content of the β-crystals reduced, compared to that of the quiescently crystallized β-nucleated iPP. It was due to the existence of abundant α-nuclei (about 10^{16} nuclei/m^3), which was in the same order of magnitude of β-nuclei induced by the presence of β-nucleating agent. In the growth process, as the chosen temperature (134 °C) was more favorable for β-crystal growth than for α-crystal growth, the content of β-crystals was still dominant, but it was less than that from the quiescent isothermal crystallization of β-nucleated iPP. As the shear rate increased, more α-nuclei emerged, so that α-crystals increased, resulting in the further decrease of β-crystals. The in-situ SAXS results demonstrated that in the case of combined effects of shear and β-nucleating agent the stacking manner of oriented and β-nucleated molecular chains was changed, so that the long period of sheared, β-nucleated iPP was almost equivalent to that of the quiescently crystallized pure iPP. The understanding of the counteraction mechanism between shear and β-nucleating agent shall allows us to control the content of β-crystals. For example, this knowledge has offered a new pathway to manipulate the structures and properties of iPP, e.g., formation of bamboo-like bionic structure.[38] The future work will include the fine-tuning of iPP structure utilizing this strategy to simultaneously realize high strength and high toughness in the final products.

Acknowledgment. The authors are indebted to Drs. Lixia Rong and Jie Zhu from Synchrotron Light Source, Brookhaven National Laboratory (USA), for their help of WAXD and SAXS measurements. The Chinese team thanks the financial support by the National Outstanding Youth Foundation of China (Grant No. 50925311) and the National Science Foundation of China (Grant No. 20876099), and the US team thanks financial support by the National Science Foundation of the US (DMR-0906512).

References and Notes

(1) (a) Padden, F. J.; Keith, H. D. *J. Appl. Phys.* **1959**, *30*, 1479. (b) Keith, H. D.; Padden, F. J.; Walter, N. M.; Wyckoff, H. W. *J. Appl. Phys.* **1959**, *30*, 1485.
(2) Turner Jones, A.; Aizlewood, J. M.; Beckett, D. R. *Makromol. Chem.* **1964**, *75*, 134.
(3) Bruckner, S.; Meille, S. V.; Petraccone, V.; Pirozzi, B. *Prog. Polym. Sci.* **1991**, *16*, 361.
(4) Lotz, B.; Wittmann, J. C.; Lovinger, A. J. *Polymer* **1996**, *37*, 4979.
(5) Leugering, H. J. *Makromol. Chem.* **1967**, *109*, 204.
(6) (a) Shi, G.; Zhang, X.; Qiu, Z. *Makromol. Chem.* **1992**, *193*, 583. (b) Shi, G.; Chang, X.; Cao, Y.; Hong, J. *Makromol. Chem.* **1993**, *194*, 269. (c) Li, J. X.; Cheung, W. L.; Jia, D. *Polymer* **1999**, *40*, 1219. (d) Li, J. X.; Cheung, W. L. *Polymer* **1999**, *40*, 2085.
(7) (a) Ferro, D. R.; Meille, S. V.; Brückner, S. *Macromolecules* **1998**, *31*, 6926. (b) Varga, J.; Mudra, I.; Ehrenstein, G. W. *J. Appl. Polym. Sci.* **1999**, *74*, 2357.
(8) Ikeda, N.; Kobayashi, T.; Killough, L. Polypropylene '96. World Congress, Zurich, Switzerland, Sept 18−20, **1996**.
(9) Mathieu, C.; Thierry, A.; Wittmann, J. C.; Lotz, B. *J. Polym. Sci., Part B: Polym. Phys.* **2002**, *40*, 2504.
(10) Fujiwara, Y. *Colloid Polym. Sci.* **1975**, *253*, 273.
(11) Lovinger, A. J.; Chua, J. O.; Gryte, C. C. *J. Polym. Sci., Polym. Phys. Ed.* **1977**, *15*, 641.
(12) Leugering, H. J.; Kirsch, G. *Angew. Makromol. Chem.* **1973**, *33*, 17.
(13) Devaux, E.; Chabert, B. *Polym. Commun.* **1991**, *32*, 464.
(14) Varga, J.; Karger-Kocsis, J. *J. Polym. Sci., Part B: Polym. Phys.* **1996**, *34*, 657.
(15) Somani, R. H.; Hsiao, B. S.; Nogales, A.; Fruitwala, H.; Srinivas, S.; Tsou, A. H. *Macromolecules* **2001**, *34*, 5902.
(16) Tjong, S. C.; Shen, J. S.; Li, R. K. Y. *Scr. Metall. Mater.* **1995**, *33*, 503.
(17) (a) Karger-Kocsis, J.; Varga, J. *J. Appl. Polym. Sci.* **1996**, *62*, 291. (b) Karger-Kocsis, J.; Varga, J.; Ehrenstein, G. W. *J. Appl. Polym. Sci.* **1997**, *64*, 2059.
(18) Chen, H. B.; Karger-Kocsis, J.; Wu, J. S.; Varga, J. *Polymer* **2002**, *43*, 6505.
(19) (a) Brückner, S.; Meille, S. V. *Nature* **1989**, *340*, 455. (b) Meille, S. V.; Brückner, S.; Porzio, W. *Macromolecules* **1990**, *23*, 4114.
(20) Norton, D. T.; Keller, A. *Polymer* **1985**, *26*, 704.
(21) Jin, Y.; Hiltner, A.; Baer, E.; Masirek, R.; Piorkowska, E.; Galeski, A. *J. Polym. Sci., Part B: Polym. Phys.* **2006**, *44*, 1795.
(22) Grein, C. *Adv. Polym. Sci.* **2005**, *188*, 43.
(23) Galli, P.; Vecellio, G. *Prog. Polym. Sci.* **2001**, *26*, 1287.
(24) Bucknall, C. B.; Soares, V. L. P.; Yang, H. H.; Zhang, X. C. *Macromol. Symp.* **1996**, *101*, 265.
(25) Karnani, R.; Krishnan, M.; Narayan, R. *Polym. Eng. Sci.* **1997**, *37*, 476.
(26) Thio, Y. S.; Argon, A. S.; Cohen, R. E.; Weinberg, M. *Polymer* **2002**, *43*, 3661.
(27) Stocker, W.; Schumacher, M.; Graff, S.; Thierry, A.; Wittmann, J. C.; Lotz, B. *Macromolecules* **1998**, *31*, 807.
(28) Zhou, J. J.; Liu, J. G.; Yan, S. K.; Dong, J.; Y.; Li, L.; Chan, C. M.; Schultz, J. M. *Polymer* **2005**, *46*, 4077.
(29) Scudla, J.; Raab, M.; Eichhorn, K. J.; Strachota, A. *Polymer* **2003**, *44*, 4655.
(30) Chvatalova, L.; Navratilova, J.; Cermak, R.; Raab, M.; Obadal, M. *Macromolecules* **2009**, *42*, 7413.
(31) Horváth, Zs.; Sajó, I. E.; Stoll, K.; Menyhárd, A.; Varga, J. *eXPRESS Polym. Lett.* **2010**, *4*, 101.
(32) Dong, M.; Gou, Z. X.; Yu, J.; Su, Z. Q. *J. Polym. Sci., Part B: Polym. Phys.* **2008**, *46*, 1725.
(33) Varga, J.; Menyhárd, A. *Macromolecules* **2007**, *40*, 2422.
(34) Bai, H. W.; Wang, Y.; Zhang, Z. J.; Han, L.; Li, Y. L.; Liu, L.; Zhou, Z. W.; Men, Y. F. *Macromolecules* **2009**, *42*, 6647.
(35) Zhang, C. G.; Hu, H. Q.; Wang, D. J.; Yan, S.; Han, C. C. *Polymer* **2005**, *46*, 8157.
(36) Varga, J. *J. Therm. Anal.* **1989**, *35*, 1891.
(37) Huo, H.; Jiang, S. J.; An, L. J.; Feng, J. C. *Macromolecules* **2004**, *37*, 2478.
(38) Chen, Y. H.; Zhong, G. J.; Wang, Y.; Li, Z. M.; Li, L. B. *Macromolecules* **2009**, *42*, 4343.
(39) Turner Jones, A.; Cobbold, A. *J. Polym. Lett.* **1968**, *6*, 539.
(40) Kumaraswamy, G.; Kornfield, J. A.; Yeh, F. J.; Hsiao, B. S. *Macromolecules* **2002**, *35*, 1762.
(41) Zhao, S. C.; Cai, Z.; Xin, Z. *Polymer* **2008**, *49*, 2745.
(42) De-Rosa, C.; Napolitani, R.; Pizozzi, B. *Eur. Polym. J.* **1984**, *20*, 937.

(43) Meille, S. V.; Ferro, D. R.; Brückner, S.; Lovinger, A. J.; Padden, F. J. *Macromolecules* **1994**, *27*, 2615.
(44) Nogales, A.; Mitchell, G. R. *Polymer* **2005**, *46*, 5615.
(45) Haeringen, D. T.; Varga, J.; Ehrenstein, G. W.; Vancso, G. J. *J. Polym. Sci., Part B: Polym. Phys.* **2000**, *38*, 672.
(46) Somani, R. H.; Hsiao, B. S.; Nogales, A.; Srinivas, S.; Fruitwala, H.; Tsou, A. H.; Sics, I.; Balta-Calleja, F. J.; Ezquerra, T. A. *Macromolecules* **2000**, *33*, 9385.
(47) Kalay, G.; Bevis, M. J. *J. Polym. Sci., Part B: Polym. Phys.* **1997**, *35*, 241.
(48) Housmans, J. W.; Gahleitner, M.; Peters, G. W. M.; Meijer, H. E. H. *Polymer* **2009**, *50*, 2304.
(49) (a) Kornfield, J. A.; Kumaraswamy, G.; Issaian, A. M. *Ind. Eng. Chem. Res.* **2002**, *41*, 6383. (b) Kimata, S.; Sakurai, T.; Nozue, Y.; Kasahara, T.; Yamaguchi, N.; Karino, T.; Shibayama, M.; Kornfield, J. A. *Science* **2007**, *316*, 1014. (c) Rendon, S.; Burghardt, W. R.; Auad, M. L.; Kornfield, J. A. *Macromolecules* **2007**, *40*, 6624.
(50) (a) Hsiao, B. S.; Yang, L.; Somani, R. H.; Avila-Orta, C. A.; Zhu, L. *Phys. Rev. Lett.* **2005**, *94*, 117802. (b) Keum, J. K.; Zuo, F.; Hsiao, B. S. *Macromolecules* **2008**, *41*, 4766. (c) Larin, B.; Avila-Orta, C. A.; Somani, R. H.; Hsiao, B. S.; Marom, G. *Polymer* **2008**, *49*, 295.
(51) (a) Hwang, W. R.; Peters, G. W. M.; Hulsen, M. A.; Meijer, H. E. H. *Macromolecules* **2006**, *39*, 8389. (b) Van der Beek, M. H. E.; Peters, G. W. M.; Meijer, H. E. H. *Macromolecules* **2006**, *39*, 9278. (c) Tufano, C.; Peters, G. W. M.; Meijer, H. E. H. *Langmuir* **2008**, *24*, 4494.
(52) (a) Elmoumni, A.; Winter, H. H. *Rheol. Acta* **2006**, *45*, 793. (b) Mandare, P.; Winter, H. H. *Rheol. Acta* **2007**, *46*, 1161. (c) Siebenburger, M.; Fuchs, M.; Winter, H. H.; Ballauff, M. *J. Rheol.* **2009**, *53*, 707.
(53) (a) Braun, J.; Wippel, H.; Eder, G.; Janeschitz-Kriegl, H. *Polym. Eng. Sci.* **2003**, *43*, 188. (b) Janeschitz-Kriegl, H. *Macromolecules* **2006**, *39*, 4448. (c) Janeschitz-Kriegl, H.; Eder, G. *J. Macromol. Sci., Phys.* **2007**, *46*, 591.
(54) (a) Testa, C.; Sigillo, I.; Grizzuti, N. *Polymer* **2001**, *42*, 5651. (b) Acierno, S.; Coppola, S.; Grizzuti, N. *J. Rheol.* **2008**, *52*, 551.
(55) Lauritzen, J. I.; Hoffman, J. D. *J. Res. Natl. Bur. Stand.* **1960**, *64A*, 73.
(56) Hoffman, J. D.; Lauritzen, J. I. *J. Res. Natl. Bur. Stand.* **1961**, *65A*, 297.
(57) Byelov, D.; Panine, P.; Remerie, K.; Biemond, E.; Alfonso, G. C.; de Jeu, W. H. *Polymer* **2008**, *49*, 3076.
(58) Alfonso, G. C.; Azzurri, F. In Proceedings of the meeting polymer crystallization and structure formation in processing, Linz, Austria, Nov **2003**.
(59) Kolmogoroff, A. N. *Isv. Akad. Nauk SSSR, Ser. Math.* **1937**, *1*, 355.
(60) Avrami, M. *J. Chem. Phys.* **1939**, *7*, 1103.
(61) Varga, J. *J. Mater. Sci.* **1992**, *27*, 2557.